Preclinical Evaluation and Nonhuman Primate Receptor Occupancy Study of ^{18}F-JNJ-64413739, a PET Radioligand for P2X7 Receptors

Hartmuth C. Kolb[1], Olivier Barret[2], Anindya Bhattacharya[1], Gang Chen[1], Cristian Constantinescu[2], Chaofeng Huang[1], Michael Letavic[1], Gilles Tamagnan[2], Chunfang A. Xia[1], Wei Zhang[1], and Anna Katrin Szardenings[1]

[1]*Janssen Research and Development LLC, San Diego, California; and* [2]*MNI, a Division of Invicro, New Haven, Connecticut*

The P2X7 receptor is an adenosine triphosphate–gated ion channel, which is abundantly expressed in glial cells within the central nervous system and in the periphery. P2X7 receptor activation leads to the release of the proinflammatory cytokine IL-1β in the brain, and antagonism of the P2X7 receptor is a novel therapeutic strategy to dampen adenosine triphosphate–dependent IL-1β signaling. PET ligands for the P2X7 receptor will not only be valuable to assess central target engagement of drug candidates but also hold promise as surrogate markers of central neuroinflammation. Herein we describe the in vitro and in vivo evaluation of ^{18}F-JNJ-64413739, an ^{18}F-labeled PET ligand for imaging the P2X7 receptor in the brain. **Methods:** P2X7 receptor affinity and specificity, pharmacokinetics, metabolic stability, blood–brain barrier permeability, and off-target binding of JNJ-64413739 were evaluated in a series of in vitro, ex vivo, and in vivo assays. ^{18}F-JNJ-64413739 was radiolabeled via a one-step nucleophilic aromatic substitution. The tracer was also studied in rhesus macaques, and PET images were analyzed with an arterial plasma input function–based Logan graphical analysis. **Results:** The potency (half-maximal inhibitory concentration) of the P2X7 receptor antagonist JNJ-64413739 is 1.0 ± 0.2 nM and 2.0 ± 0.6 nM at the recombinant human and rat P2X7 receptor, respectively, and the binding affinity is 2.7 nM (rat cortex binding assay) and 15.9 nM (human P2X7 receptor). In nonhuman primate PET imaging studies, dose-dependent receptor occupancy of JNJ-54175446 was observed in 2 rhesus monkeys. At a 0.1 mg/kg dose (intravenous) of JNJ-54175446, the receptor occupancy was calculated to be 17% by Logan graphical analysis, whereas a dose of 2.5 mg/kg yielded a receptor occupancy of 60%. **Conclusion:** The preclinical evaluation of ^{18}F-JNJ-64413739 demonstrates that the tracer engages the P2X7 receptor. Reproducible and dose-dependent receptor occupancy studies with the P2X7 receptor antagonist JNJ-54175446 were obtained in rhesus monkeys. This novel PET tracer exhibits in vitro and in vivo characteristics suitable for imaging the P2X7 receptor in the brain and warrants further studies in humans.

Key Words: P2X7 receptor; PET imaging; occupancy study

J Nucl Med 2019; 60:1154–1159
DOI: 10.2967/jnumed.118.212696

The P2X7 receptor belongs to the P2X family of trimeric ligand-gated cation channels, and its activation by adenosine triphosphate (ATP) allows for the flux of several cations, including Ca^{2+}, Na^{+}, and K^{+} (*1,2*). The ATP-gated purinergic P2X7 receptor is abundantly expressed in central nervous system (CNS) microglia (*3*). In the brain, the P2X7 receptor is expressed ubiquitously as demonstrated by immunohistochemistry, autoradiography and PET imaging (*4–6*). At a functional level, the P2X7 receptor is activated by high concentrations of ATP. Under normal physiologic conditions, extracellular ATP concentrations are generally below the threshold required for P2X7 receptor activation, and P2X7 receptor signaling is believed to be silent. However, during CNS pathology extracellular ATP levels can reach sufficiently high concentrations to activate the receptor, as has been demonstrated with P2X7 receptor antagonists in models of disease (*7*). Hence, whereas P2X7 receptor expression levels are detectable or high in normal CNS tissues, their ion channel activity might be low or inactive. Although expression levels may or may not be upregulated during a neuroinflammatory response, the ion channel activity will most likely be engaged in a disease state, making a case for targeting the P2X7 receptor as an attractive drug target for CNS therapeutics (*8*).

One of the features of the P2X7 receptor activation is NLRP3 inflammasome activation followed by release of proinflammatory cytokines IL-1β and IL-18 (*9*), which is dependent on 2 critical steps working in concert: a priming of toll-like receptors by lipopolysaccharide and a subsequent activation of the P2X7 receptor by ATP, such that each one on its own will be unable to trigger P2X7 receptor mediated IL-1β/IL-18 release. The release of these cytokines triggers a cascade of downstream events leading to microglial activation, astrogliosis, and ultimately neuroinflammation. Once the P2X7 receptor is activated, it also serves as a conduit for further intracellular ATP release (*10*), leading to a self-propelled increase of an inflammatory response. In animal models of neuroinflammation, such as ones induced by lipopolysaccharide, polyI:C, BCG, IFN-α, or kainic acid, it is critical to model the priming step and generate sufficient extracellular ATP to engage P2X7 receptor dependent IL-1β release in the brain. This was elegantly demonstrated by Territo et al. (*11*), who used a high-dose lipopolysaccharide (5 mg/kg) model of neuroinflammation to show enhanced brain uptake of ^{11}C-GSK1482160, a P2X7 receptor PET ligand. Likewise, in a model of multiple sclerosis, the same PET ligand was shown to have higher retention in the spinal cord (*12*), suggesting P2X7 receptor upregulation in these

Received Apr. 30, 2018; revision accepted Jan. 1, 2019.
For correspondence or reprints contact: Anna Katrin Szardenings, Janssen Research and Development LLC, 3210 Merryfield Row, San Diego, CA 92121.
E-mail: aszarden@its.jnj.com
Published online Feb. 7, 2019.

extreme conditions in rodents. Due to the intricate link of P2X7 receptor activation with IL-1β release and neuroinflammation, there is a lot of interest in developing clinical candidates that are both P2X7 receptor antagonists and PET ligands. Although the former class of molecules may be useful to treat CNS disorders with a neuroinflammatory component, PET ligands for the P2X7 receptor may serve a dual purpose: for use in the clinic as a biomarker to support central target engagement of the P2X7 receptor and for use as tools to study neuroinflammation.

We have published several classes of brain-penetrant P2X7 receptor antagonists, including our clinical compound JNJ-54175446. Our team has disclosed a ^{11}C-labeled P2X7 receptor PET ligand, JNJ-54173717 (*13*), which was successfully used to detect basally overexpressed P2X7 receptors in rat brains. In these models, the PET signal was blocked by competition with cold P2X7 receptor ligands in a dose-dependent manner. Similarly, the ^{11}C-GSK1482160 PET signal in the brain of lipopolysaccharide-challenged rats was also blocked by a cold P2X7 antagonist, demonstrating specificity of the PET signal to P2X7 receptors. In addition to ^{11}C-JNJ-54173717 and ^{11}C-GSK1482160, 2 other groups have disclosed P2X7 receptor PET ligands (^{11}C-A-7400003 and ^{18}F-EFB), albeit with no data to support target specificity of these tracers (*14,15*). Most recently, ^{11}C-SMW139 was described as a brain-permeable and selective P2X7 receptor ligand by Janssen et al., with promising results obtained in a rat model overexpressing human P2X7 receptor (*16*)

Here, we report a new P2X7 receptor PET ligand, ^{18}F-JNJ-64413739, to support our clinical therapeutic candidate, JNJ-54175446, with occupancy studies. In addition, this ligand will be used to study conditions of neuroinflammation. This article describes the radiochemistry, preclinical pharmacology, and nonhuman primate PET data in support of ^{18}F-JNJ-64413739 as a best-in-class CNS-penetrant P2X7 receptor PET ligand.

MATERIALS AND METHODS

Synthesis of precursor and standard are provided in the supplemental data (supplemental materials are available at http://jnm.snmjournals.org).

Radiochemistry

The radiotracer used in this study is a sterile, nonpyrogenic solution of no-carrier-added ^{18}F-JNJ-64413739 in a formulation solution. The radiotracer was prepared by reaction of the corresponding chloro precursor, (*S*)-(3-chloro-2-(trifluoromethyl)pyridin-4-yl)(6-methyl-1-(pyrimidin-2-yl)-6,7-dihydro-1H-[1,2,3]triazolo[4,5-c]pyridin-5(4H)-yl)methanone (JNJ-64410047), with ^{18}F fluoride in the presence of potassium carbonate and Kryptofix-222 (Fig. 1) using a commercial synthesizer, GE Healthcare TRACERlab FX-FN.

Purification was performed by reverse-phase high-performance liquid chromatography using a Phenomenex Luna C18(*2*) column (10 μm, 10 × 250 mm) eluted with a mixture of acetonitrile/water/trifluoroacetic acid (40/60/0.1, v/v/v) at a flow rate of 4 mL/min. The product fraction was collected in a flask containing 20 mL of diluted sodium ascorbic in water for injection. The diluted product mixture was passed through a solid-phase extraction cartridge (Sep-Pak C18 Light), and the cartridge was rinsed with 10 mL of diluted sodium ascorbic in water for injection. The radiolabeled product was eluted from the solid-phase extraction cartridge with 1.0 mL of 200-proof U.S. Pharmacopeia grade ethanol into the formulation flask, preloaded with 10 mL of formulation base (diluted sodium ascorbate containing polysorbate-80). The Sep-Pak cartridge was rinsed with 4 mL of formulation base, and the rinse was mixed with the contents of the formulation flask. The resulting solution was passed through a sterilizing 0.2-μm membrane filter into a sterile, filter-vented final product vial.

Quality control testing included visual inspection of appearance. Identity, chemical, and radiochemical purity were determined by high-performance liquid chromatography. Strength was measured by γ-assay. Filter integrity, pyrogen content, and sterility were determined by compendial tests per the U.S. Pharmacopeia. Residual solvents were determined by gas chromatography. pH was measured using pH paper. A total of 7 preparations with an average tracer purity of 99.8% ± 0.3% were used during this study. The average decay-corrected radiochemical yield was 3.1% ± 2.0%, and the average molar activity at the end of synthesis was 48.3 ± 22.3 GBq/μmol.

In Vitro Pharmacology: Binding Affinity, Half-Maximal Inhibitory Concentration in Humans and Rats

For in vitro functional assays on 1321N cell lines expressing either the rat or human P2X7 receptor, the agonist 2 (*3*)-*O*-(4-benzoylbenzoyl)adenosine 5-triphosphate (Bz-ATP) was used for channel activation, and JNJ-41857660 as the reference compound (pIC50, 6.3 ± 0.5). Radioligand binding experiments were conducted using ^{3}H-A804598 and 1321N1 cells expressing the recombinant human and rat P2X7 receptor. Experimental details are provided in the supplemental materials.

Microdosing Experiments in Rodents

Animals/Rodents. Animal studies were conducted in the United States in accordance with the Guide for the Care and Use of Laboratory Animals (*17*). Studies performed in Europe were in accordance with the European Communities Council Directive 2010/63/EU (*18*) and local legislation on animal experimentation. Facilities were accredited by the Association for the Assessment and Accreditation of Laboratory Animal Care. Animals were allowed to acclimate for 5 d after receipt. They were housed in accordance with institutional standards, received food and water ad libitum, and were maintained on a 12-h light/dark cycle.

To evaluate the brain biodistribution of JNJ-64413739 in rodents at a microdose level, rats (n = 3 per group) were administered a single intravenous dose of 0.03 mg/kg of JNJ-64413739 formulated in 20% (w/v) HP-β-cyclodextrin in ddH_2O, pH 7.4. A blocking experiment was performed by oral administration of the P2X7 antagonist JNJ-55308942 (*19*) (5 mg/kg) 1 h before microdosing of JNJ-64413739. At 2 time points (15 and 30 min) after microdosing, the cerebrums were collected and homogenized to analyze JNJ-64413739 levels by liquid chromatography with tandem mass spectrometry (LC-MS/MS).

P2X7 receptor knockout (KO) mice were used to measure nonspecific binding of JNJ-64413739 (*20*). The KO strain was a mixed genetic background of 129/Ola_C57BL/6_DBA/2 and was obtained under a license from JAX (catalog no. 005576). KO and strain-matched wild-type mice (n = 4 each) were dosed

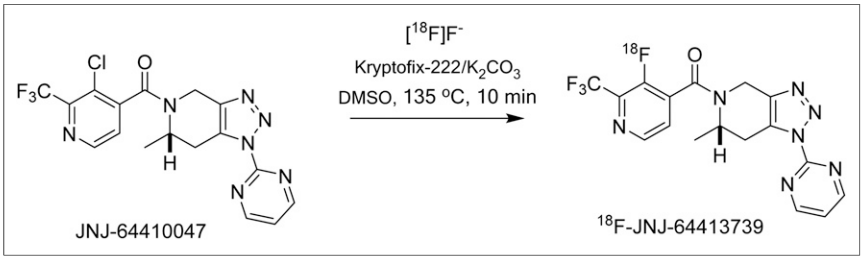

FIGURE 1. Radiosynthesis of ^{18}F-JNJ-64413739.

intravenously with JNJ-64413739 (0.1 mg/kg of body weight). Cerebrums were harvested after 30 min for LC-MS/MS analysis.

LC-MS/MS Analysis. JNJ-64413739 brain homogenate samples were extracted using a protein precipitation method and analyzed on an API4000 Q-Trap MS/MS System (Applied Biosystems, Concord, Ontario, Canada) interfaced with a Shimadzu LC high-performance liquid chromatographer. Samples were loaded onto a 2.1 × 50-mm Gemini, NX-C18, 3 μm 110A column (Phenomenex) under a flow rate of 0.5 mL/min using water (0.1% formic acid) as mobile phase A and acetonitrile (0.1% formic acid) as mobile phase B. Starting with 85% mobile phase A for 0.5 min, mobile phase B was increased from 15% to 98% using a linear gradient for 1.1 min, held at 98% B for 0.6 min, and equilibrated at 15% B for 0.4 min for an overall run time of 2.5 min. JNJ-64413739 was quantified by MS/MS in the positive ion mode by monitoring the transition of 408 to 172 m/z.

Nonhuman Primate Brain PET Imaging Studies (at MNI/Invicro)

Animals. All experiments were conducted in accordance with the U.S. Public Health Service's Policy on Humane Care and Use of Laboratory Animals and with institutional approval. Adult rhesus macaques (*Macaca mulatta*, 1 female and 1 male, 10.3 ± 2.3 kg) were used. An intravenous catheter was used for administration of fluids for hydration. Body temperature was maintained by a heated water blanket and monitored with a rectal thermometer. Vital signs were monitored continuously and recorded every 10–20 min during the study.

Vehicle and Blocking Agent. JNJ-54175446 was formulated in a vehicle of acetate buffer (100 mM, pH 4.5) containing 20% PEG400 and 20% HP-β-CD. The concentration of the solution was determined by high-performance liquid chromatography (Xbridge C18, methanol/ammonium acetate 5 mM, 70/30, 1 mL/min, 254 nm) by comparison with a 1 mg/mL standard solution in dimethyl sulfoxide. Vehicle only or JNJ-54175446 at doses of 0.1, 0.4, 2.5 (duplicate) and 5.3 mg/kg were administered intravenously over 3 min, starting 10 min before tracer injection. Blood samples were taken at −5 (predose), 10, 20, 40, 70, 100, and 130 min relative to the start of JNJ-54175446 injection to measure its plasma levels during PET imaging.

PET Acquisition. PET scans (n = 7) were performed on a Focus 220 small-animal PET camera (Siemens Healthcare Molecular Imaging) after intravenous administration of 179.8 ± 9.9 MBq of ^{18}F-JNJ-64413739: 2 scans with vehicle only and 5 scans after blocking with JNJ-54175446. PET images were acquired over a period of 2 h. The dynamic series was reconstructed using filtered backprojection with corrections for randoms, scatter, and attenuation.

Arterial Input Function. Arterial blood samples were collected over 2 h after tracer administration. Radioactivity in whole blood and plasma were measured in all samples. A subset of plasma samples was processed by acetonitrile denaturation, and radiometabolites and parent fractions were measured by reverse-phase high-performance liquid chromatography performed on a Phenomenex Luna C18(2) (10 × 250 mm, 10 μm) column eluted with a mobile phase consisting of a mixture of methanol/water with 0.2% triethylamine in a 65/35 ratio at a flow rate of 4 mL/min. Plasma radioactivity and parent fraction curves were used to generate the metabolite-corrected arterial input function. The plasma protein binding free fraction was measured by ultrafiltration (Centrifree; Millipore).

Image Processing. PET images were analyzed in PMOD 3.6 (PMOD Technologies) and were motion-corrected when necessary. The first postvehicle image of each primate was normalized to an MR rhesus brain template (*21*). Subsequent images of the same primate were coregistered to their corresponding vehicle image, thus transforming each image to a standard space. A volume-of-interest atlas template including multiple brain regions with variable tracer uptake was applied to the PET images, and time–activity curves of the average activity concentration over time within each region were generated. Time–activity curves were expressed in SUV units (g/mL) by normalizing by the weight of the animal and the injected dose.

TABLE 1
IC_{50} and K_i Values for JNJ-64413739 (Mean ± SD)

Assay	JNJ-64413739
IC_{50} P2X7 human (nM)	1.0 ± 0.2
IC_{50} P2X7 rat (nM)	2.0 ± 0.6
K_i P2X7 human (nM)	15.9 ± 2.0
K_i P2X7 rat (nM)	2.7 ± 1.1

IC_{50} = half-maximal inhibitory concentration; K_i = binding affinity.

Kinetic Modeling and Analysis. All kinetic analyses were performed using PMOD 3.6. The plasma-based Logan graphical analysis (*22*), with a cutoff t* fixed at 20 min, was applied to the regional time–activity curves using the arterial plasma input function corrected for radiometabolites to determine the total volume of distribution V_T for each brain region (*23*). No region in the brain devoid of P2X7 receptor could be identified, and the occupancy at each JNJ-54175446 dose was estimated using the global occupancy plot (*24*), with $V_T^{Baseline} - V_T^{JNJ446}$ on the y-axis and $V_T^{Baseline}$ on the x-axis, where $V_T^{Baseline}$ is the V_T at baseline, and V_T^{JNJ446} is the V_T after JNJ-54175446 administration. The occupancy is given by the slope of the linear regression, and the nondisplaceable distribution volume, V_{ND}, is given by the x-intercept.

RESULTS

In Vitro Pharmacology

The potency (half-maximal inhibitory concentration) of JNJ-64413739 is 1.0 ± 0.2 nM (n = 3, recombinant human P2X7 receptor) and 2.0 ± 0.6 nM (n = 3, recombinant rat P2X7 receptor), and the binding affinity is 2.7 nM (1.7, 3.8) in a rat cortex binding assay and 15.9 nM (*14*, *18*) for the human P2X7 receptor (Table 1). In vitro microsomal stability testing suggested excellent

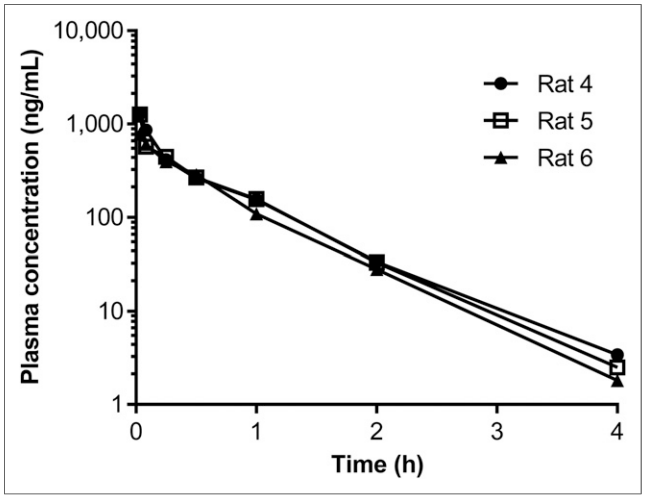

FIGURE 2. Rat intravenous pharmacokinetics profile: time vs. plasma concentration of JNJ-64413739 (n = 3).

TABLE 2
Rat Intravenous Pharmacokinetics Parameters of JNJ-64413739

Rat no.	CL (mL/min/kg)	CL (L/h/kg)	V_d (L/kg)	V_{ss} (L/kg)	AUC_{INF} (h*ng/mL)	C_0 (ng/mL)	C_0 (μM)	Half-life, terminal (h)
4	33.6	2.0	1.6	1.3	497	1660	4.1	0.6
5	34.8	2.1	1.5	1.3	479	2119	5.2	0.5
6	41.6	2.5	1.8	1.6	401	921	2.3	0.5
Mean	36.6	2.2	1.7	1.4	459	1567	3.8	0.5
SD	4.3	0.3	0.2	0.1	51	604	1.5	0.0
%CV	12	12	9	11	11	39	39	5

CL = clearance; V_d = volume of distribution; V_{ss} = apparent volume of distribution at steady state; AUC_{INF} = area under the curve extrapolated to infinite time; C_0 = extrapolated plasma concentration at time 0; %CV = percentage coefficient of variation.

metabolic stability in humans (half-life = 180 min) and rats (half-life > 60 min). Human plasma protein binding was determined to be 63% (free fraction), and the free fraction in rat brain tissue was 19%, which are in an acceptable range for a PET ligand (*25*).

Pharmacokinetics and Metabolism in Rats

Absorption and Pharmacokinetics. An MDR1-MDCK permeability assay (P-glycoprotein substrate identification) was performed to assess CNS permeability of the compound and to characterize whether it is a P-glycoprotein substrate. The efflux ratio was determined to be 13.8. To determine the pharmacokinetic profile of this antagonist, a single intravenous dose of JNJ-64413739 at 1 mg/kg was administered to male SD rats (n = 3). Plasma levels were determined at different time-points for 4 h after dosing (Fig. 2).

A maximum plasma concentration of 1,107 ng/mL was reached at 2 min after injection. The area under the curve to infinity was determined to be 459 h·ng/mL with a clearance of 36.6 mL/min/kg (Table 2).

The blood–brain barrier permeability of JNJ-64413739 was assessed by administering the compound intravenously at 1 mg/kg to male SD rats. The concentrations of JNJ-64413739 in plasma and brain homogenate were measured at different time points after dosing (Fig. 3). The brain-to-plasma ratio was 0.8 at 5 min, 0.91 at 30 min, 0.92 at 60 min, and 1.08 at 120 min after injection, respectively.

Microdosing Experiments. For microdosing/blocking experiments with JNJ-64413739 (0.03 mg/kg, intravenous dosing) in rats, all animals (n = 3 per group) were pretreated orally with the P2X7 antagonist JNJ-55308942 (5 mg/kg or vehicle) 1 h before administration of JNJ-64413739. Brain uptake of JNJ-64413739 in the pretreatment group decreased by 42.3% (15 min) and 43.7% (30 min) compared with the control group (vehicle only, n = 3) (Fig. 4). In a microdosing experiment with JNJ-64413739 (0.1 mg/kg, intravenous dosing) in wild-type and P2X7 receptor KO mice, compound levels in the brains of KO mice (n = 4) after 30 min were 38% lower than that in wild-type mice (Fig. 5).

PET Imaging in Rhesus Monkeys. In vivo PET studies in rhesus macaque monkeys confirmed rapid brain uptake peaking within 10 min (up to 1.5 to 2 SUVs in cortical and subcortical regions, and cerebellar cortex), slowly clearing from the brain over the next 2 h (Fig. 6). The diffuse distribution of the signal in the brain was consistent with the known wide-spread distribution of the P2X7 receptor in astrocytes and microglia, which also precluded identification of a reference region for modeling and quantifying the tracer uptake using brain tissue activity alone. The V_T of the signal could be readily estimated from graphical analysis of the tissue curves using the arterial input function, and arterial sampling is planned in the initial studies in humans.

^{18}F-JNJ-64413739 was stable in blood ex vivo and showed good metabolic stability in vivo, with 40% and 20% of parent tracer remaining at 30 and 120 min after injection, respectively, with a high protein-binding free fraction in plasma of 72.3% ± 2.5%

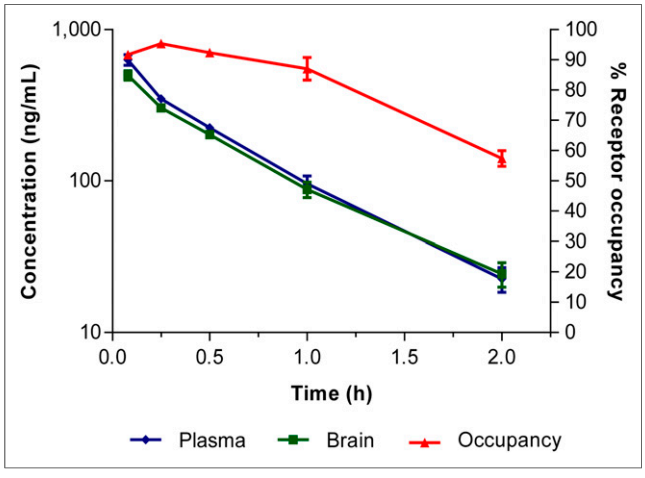

FIGURE 3. Brain vs. plasma concentration of JNJ-64413739 in rats (n = 3) over time.

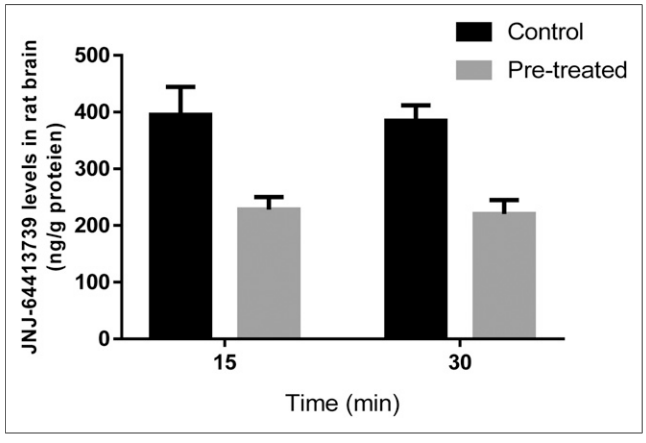

FIGURE 4. Microdosing blocking of retention of JNJ-64413739 in rat brain pretreated with JNJ-55308942 or vehicle (n = 3 each). *P < 0.01 vs. control.

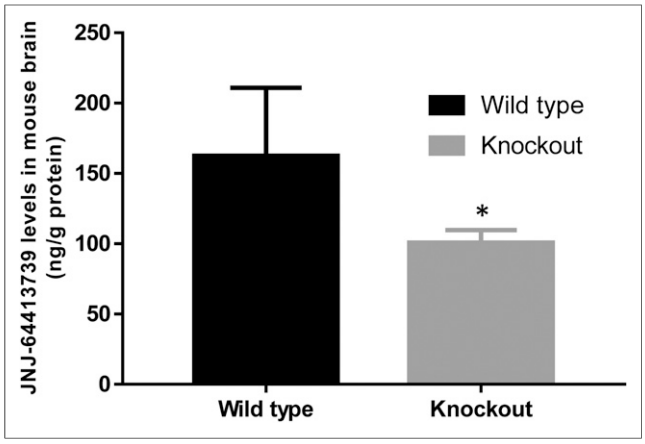

FIGURE 5. Brain uptake/retention of JNJ-64413739 in wild-type and KO mice (n = 4 each). *$P < 0.05$ vs. wild-type.

(n = 7). ^{18}F-JNJ-64413739 metabolism was not altered by the presence of JNJ-54175446. Signal accumulation in bone was not observed (no defluorination), suggesting this will not confound quantitation of the ^{18}F-JNJ-64413739 brain signal. ^{18}F-JNJ-64413739 V_T values computed with Logan graphical analysis after vehicle ranged from about 1.7 in the cerebellar cortex to about 2.4–2.7 in the thalamus. The global brain distribution of ^{18}F-JNJ-64413739 was reduced in a dose-dependent manner by pretreatment with 0.1 (~18% occupancy) to 5 mg/kg (>50% occupancy) JNJ-54175446 intravenously in rhesus monkey (Table 3). Dose dependency of ^{18}F-JNJ-64413739 binding to the P2X7 receptor is demonstrated in Figure 6 by comparing the time–activity curves acquired in the vehicle study with the JNJ-54175446 pretreatment studies at different doses.

Occupancy estimates for both monkeys plateaued at around 55%. At highest doses, V_T was reduced and ranged from about 1.5 in the cerebellar cortex to about 1.8 in the thalamus, whereas from the occupancy plots, the V_{ND} was estimated at 1.2 ± 0.1. This indicates a certain level of nonspecific binding of ^{18}F-JNJ-64413739.

DISCUSSION

The study characterizes a novel ^{18}F-fluorinated P2X7 receptor antagonist PET ligand, JNJ-64413739. P2X7 receptors are abundantly expressed in brain microglia and are a potential drug target for neuroinflammatory disorders. The Janssen team has recently disclosed 2 clinical candidates, JNJ-54175446 (*4*) and JNJ-55308942 (*18*), both of which are CNS-penetrant P2X7 receptor antagonists. In CNS drug development, unequivocal demonstration of central target engagement in both human subjects (phase 1) and patients (phase 2) are critical in dose selection during pivotal proof-of-concept studies. The preclinical studies described here in detail demonstrate that ^{18}F-JNJ-64413739 is a PET ligand that binds to the P2X7 receptor at the same site as JNJ-54175446 and JNJ-55308942 and will be a critical tool in demonstrating human brain binding of our P2X7 receptor clinical compounds.

JNJ-64413739 is a potent (half-maximal inhibitory concentration, 1 nM; binding affinity, 16 nM human P2X7 receptor) antagonist. Brain uptake and selectivity of the cold compound were assessed by MS/MS analysis of brain tissues in rats in blocking experiments and in a KO mouse model. Brain-to-plasma ratios in rats are close to 1 and brain uptake is moderate. Microdosing blocking experiments and residual binding in the KO mouse model suggest a certain degree of nonspecific binding of this tracer in brain tissue. However, since the animals used in these experiments had no neuroinflammatory pathology, baseline levels and activity of the target can also be expected to be generally low. The evaluation of ^{18}F-JNJ-64413739 in neuroinflammatory models will be reported in due course elsewhere. Occupancy studies in rhesus monkeys plateaued at 55%–60% at the highest doses, which agrees with the findings in rodents. However, the PET signal was blocked in a dose-dependent manner and the tracer showed excellent metabolic stability with little protein binding. No bone uptake was observed. The findings encourage us to move forward with ^{18}F-JNJ-64413739 to measure occupancies of the therapeutic JNJ-54175446 in the clinic.

PET displacement data shown in monkeys usually closely mirror human data, providing confidence that data obtained from monkey brain using PET imaging can be used with a high degree of translational validity. In addition to using ^{18}F-JNJ-64413739 as a clinical imaging agent to aid in P2X7 receptor drug development efforts, P2X7 receptor PET ligands may also offer new hope in probing

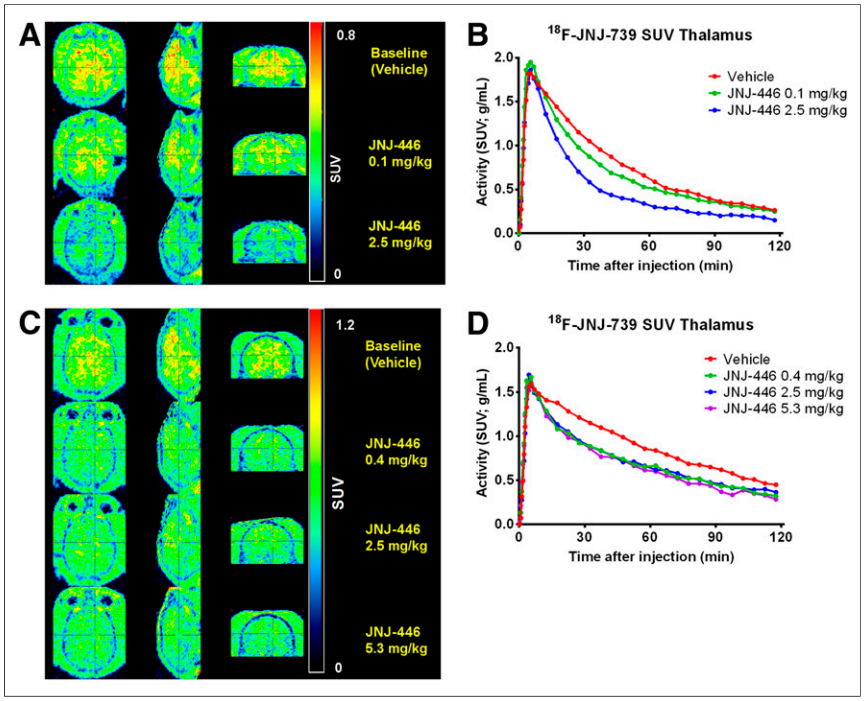

FIGURE 6. ^{18}F-JNJ-64413739 NHP PET: blocking with P2X7 inhibitor JNJ-54175446. Summed images at 30–120 min normalized to SUV acquired after either vehicle or JNJ-54175446 at different dose levels are shown for monkey 1 (A) and monkey 2 (C). Corresponding time–activity curves of thalamus expressed as SUV are shown for monkey 1 (B) and monkey 2 (D). JNJ-739 = JNJ-64413739; JNJ-446 = JNJ-54175446.

TABLE 3
Target Occupancy of JNJ-54175446 in Nonhuman Primates

Dose (mg/kg)	AUC (ng/mL × min)	Receptor occupancy (%)	Monkey
5.3	132470	51.7	2
2.5	46991	60.4	1
2.5	42353	55.1	2
0.4	5764	52.1	2
0.1	2102	17.6	1

AUC = area under the curve.

CNS microglial activation. TSPO remains the only marker of microglial activation so far, and there have been numerous reports and reviews of TSPO PET ligands (*26*). P2X7 receptor PET imaging may offer a unique opportunity to compare TSPO PET signals from patients with neurodegeneration and neuropsychiatric illnesses. Based on the role of P2X7 receptors in neuroinflammation, there is hope that P2X7 receptor PET may complement, if not replace, TSPO PET ligands, which have shown limitations in the clinic due to polymorphism and high signal-to-noise ratios (*27*). P2X7 receptor upregulation in neuroinflammation is subtle and thereby high-affinity PET ligands may be useful for patient stratification.

CONCLUSION

^{18}F-JNJ-64413739 behaves as a suitable PET ligand for the P2X7 receptor and has shown dose-dependent competitive binding with JNJ-54175446 in monkey PET studies in vivo. It therefore could be a useful PET ligand for receptor occupancy studies in humans.

DISCLOSURE

Anindya Bhattacharya, Gang Chen, Chaofeng Huang, Hartmuth Kolb, Michael Letavic, Anna Szardenings, Chunfang Xia, and Wei Zhang are employed by Janssen, who provided financial support for this research project. Olivier Barret, Cristian Constantinescu, and Gilles Tamagnan were employed by MNI, Molecular Neuroimaging, LLC, now Invicro, who were contracted by Janssen to perform the nonhuman primate studies. No other potential conflict of interest relevant to this article was reported.

ACKNOWLEDGMENTS

We thank Brian Lord for generating pharmacokinetics and occupancy data in rats, Hong Ao for determining half-maximal inhibitory concentrations and binding affinity, and Leslie Nguyen for performing pharmacokinetic analysis of the microdosing samples.

REFERENCES

1. Bartlett R, Stokes L, Sluyter R. The P2X7 receptor channel: recent developments and the use of p2x7 antagonists in models of disease. *Pharmacol Rev.* 2014;66:638–675.
2. Sperlágh B, Illes P. P2X7 receptor: an emerging target in central nervous system diseases. *Trends Pharmacol Sci.* 2014;35:537–547.
3. Bhattacharya A, Biber K. The microglial ATP-gated ion channel P2X7 as a CNS drug target. *Glia.* 2016;64:1772–1787.
4. Letavic MA, Savall BM, Allison BD, et al. 4-Methyl-6,7-dihydro-4H-triazolo[4,5-c]pyridine-based P2X7 receptor antagonists: optimization of pharmacokinetic properties leading to the identification of a clinical candidate. *J Med Chem.* 2017;60:4559–4572.
5. Lord B, Ameriks MK, Wang Q, et al. A novel radioligand for the ATP-gated ion channel P2X7: [^{3}H] JNJ-54232334. *Eur J Pharmacol.* 2015;765:551–559.
6. Ory D, Celen S, Gijsbers R, et al. Preclinical evaluation of a P2X7 receptor-selective radiotracer: PET studies in a rat model with local overexpression of the human P2X7 receptor and in nonhuman primates. *J Nucl Med.* 2016;57:1436–1441.
7. Chrovian CC, Rech JC, Bhattacharya A, et al. P2X7 antagonists as potential therapeutic agents for the treatment of CNS disorders. *Prog Med Chem.* 2014;53:65–100.
8. Rech JC, Bhattacharya A, Letavic MA, et al. The evolution of P2X7 antagonists with a focus on CNS indications. *Bioorg Med Chem Lett.* 2016;26:3838–3845.
9. He Y, Taylor N, Fourgeaud L, Bhattacharya A. The role of microglial P2X7: modulation of cell death and cytokine release. *J Neuroinflammation.* 2017;14:135–147.
10. Cisneros-Mejorado A, Perez-Samartin A, Gottlieb M, et al. ATP signaling in brain: release, excitotoxicity and potential therapeutic targets. *Cell Mol Neurobiol.* 2015;35:1–6.
11. Territo PR, Meyer JA, Peters JS, et al. Characterization of [^{11}C]-GSK1482160 for targeting the P2X7 receptor as a biomarker for neuroinflammation. *J Nucl Med.* 2017;58:458–465.
12. Han J, Liu H, Liu C, et al. Pharmacologic characterizations of a P2X7 receptor-specific radioligand, [^{11}C]GSK1482160 for neuroinflammatory response. *Nucl Med Commun.* 2017;38:372–382.
13. Ory D, Celen S, Gijsbers R, et al. Preclinical evaluation of a P2X7 receptor-selective radiotracer: PET studies in a rat model with local overexpression of the human P2X7 receptor and in nonhuman primates. *J Nucl Med.* 2016;57:1436–1441.
14. Fantoni ER, Dal Ben D, Falzoni S, et al. Design, synthesis and evaluation in an LPS rodent model of neuroinflammation of a novel ^{18}F-labelled PET tracer targeting P2X7. *EJNMMI Res.* 2017;7:31–42.
15. Janssen B, Vugts DJ, Funke U, et al. Synthesis and initial preclinical evaluation of the P2X7 receptor antagonist [(^{11}C]A-740003 as a novel tracer of neuroinflammation. *J Labelled Comp Radiopharm.* 2014;57:509–516.
16. Janssen B, Vugts DJ, Wilkinson SM, et al. Identification of the allosteric P2X7 receptor antagonist [^{11}C]SMW139 as a PET tracer of microglial activation. *Sci Rep.* 2018;8:6580.
17. National Research Council. *Guide for the Care and Use of Laboratory Animals*, 8th ed, The National Academies Press, Washington, DC. 2011.
18. European Union: *Directive 2010/63/EU of the European parliament and of the council of 22 September 2010 on the protection of animals used for scientific purposes*. *Official Journal of the European Union: L* 276:33–79.
19. Chrovian CC, Soyode-Johnson A, Peterson AA, et al. A dipolar cycloaddition reaction to access 6-methyl-4,5,6,7-tetrahydro-^{1}H-[1,2,3]triazolo[4,5-c]pyridines enables the discovery synthesis and preclinical profiling of a P2X7 antagonist clinical candidate. *J Med Chem.* 2018;61:207–223.
20. Labasi JM, Petrushova N, Donovan C, et al. Absence of the P2X7 receptor alters leukocyte function and attenuates an inflammatory response. *J Immunol.* 2002;168:6436–6445.
21. Rohlfing T, Kroenke CD, Sullivan EV, et al. The INIA19 Template and NeuroMaps Atlas for Primate Brain Image Parcellation and Spatial Normalization. *Front Neuroinform.* 2012;6:27.
22. Logan J. A review of graphical methods for tracer studies and strategies to reduce bias. *Nucl Med Biol.* 2003;30:833–844.
23. Innis RB, Cunningham VJ, Delforge J, et al. Consensus nomenclature for in vivo imaging of reversibly binding radioligands. *J Cereb Blood Flow Metab.* 2007;27:1533–1539.
24. Cunningham VJ, Rabiner EA, Slifstein M, et al. Measuring drug occupancy in the absence of a reference region: the Lassen plot re-visited. *J Cereb Blood Flow Metab.* 2010;30:46–50.
25. Zhang L, Villalobos A, Beck EM, et al. Design and Selection Parameters to Accelerate the Discovery of Novel Central Nervous System Positron Emission Tomography (PET) Ligands and Their Application in the Development of a Novel Phosphodiesterase 2A PET Ligand. *J Med Chem.* 2013;56:4568–4579.
26. Alam MM, Lee J, Lee SY. Recent progress in the development of TSPO PET ligands for neuroinflammation imaging in neurological diseases. *Nucl Med Mol Imaging.* 2017;51:283–296.
27. Vivash L, O'Brien TJ. Imaging microglial activation with TSPO PET: lighting up neurologic diseases? *J Nucl Med.* 2016;57:165–168.